On the lift curve slope for rectangular flat plate wings at moderate Reynolds number

Paloma Gutierrez-Castillo[a,*], Jorge Aguilar-Cabello[a], Sergio Alcalde-Morales[a], Luis Parras[a], Carlos del Pino[a]

[a] *Universidad de Málaga, Escuela de Ingenierías Industriales. C/ Dr. Ortiz Ramos S/N, 29071, Málaga, Spain.*

Abstract

The lift coefficient for a flat plate at low angles of attack is obtained experimentally for various aspect ratios ($AR = 1, 2, 4, 8$) and moderate Reynolds numbers ($Re = 40\times10^3$ to $Re = 200\times10^3$). The variation of the lift coefficient with the angle of attack in the pre-stall region is consistent with a linear slope approximation. We consider that this slope is a function of both the aspect ratio and Reynolds number. In this research, we provide a correlation that can predict the lift slope value with an average error of less than 5%. This correlation captures the idea of Prandtl's finite wing theory and extends its application for any Reynolds number. The same correlation is tested against other literature experiments providing very accurate results even outside our range of measured *AR* and *Re*.

Keywords: `Lift Coefficient, Rectangular Flat Plate, Low Reynolds number, Aspect Ratio`

1. Introduction

Research in wing models to study the aerodynamic characteristics is one of the principal pillars of aeronautical and aerospace engineering. Historically interested in high chord-based Reynolds numbers (*Re*) for their usual applications, the increasing use of fixed-wing unmanned and micro aerial vehicles for which *Re* of operation are significantly lower has impulsed the interest on the research of wing aerodynamics at moderate Reynolds numbers [1, 2, 3]. The results predicted by potential theory starts to fail in the range of $Re\sim O(10^4)$-$O(10^5)$. Besides, the influence of the aspect ratio (*AR*, defined as the ratio of the wingspan length over the chord of the wing) on the aerodynamic characteristics of finite wings [4, 5, 6] is of great interest even at ultra-low *Re* [7]. Typical aspect ratios are in the range of $AR \sim 2-4$, so the three-dimensional effect of the wingtip vortex plays a significant role in affecting the performance of the airfoil [8, 9]. The huge impact of these two main parameters (*Re* and *AR*) on wing models is still an open challenge in aerodynamics.

One of the simplest models of wings used as a reference for the study of aerodynamic characteristics is the rectangular flat plate [10], tested even at ultra-low Reynolds numbers [11]. Since

*Corresponding author
Email address: `paloma_gutierrez@uma.es` (Paloma Gutierrez-Castillo)

the early 20th century, the flat plate has been used to estimate the lift with bounded parallel walls to mimic the wind tunnel configuration, finding that the corrections of lift for a flat plate and aerofoil are almost identical at small incidence angles [12]. Later, lift corrections at the zero thickness limit were reported for an elliptic cylinder [13]. Interest in flat plates has not diminished since then, and it has been used as a test case for many applications at low *Re* in different areas of research. Some of the most direct applications relate to imitating a pair of winglets [14], to simulate a cascade of blades [15] or to study the stability of fluttering [16]. Others are inspired by the small flyers present in nature, such as comparing rigid and membrane wing models [17], analyzing pitching movements [18], or finding bio-inspired corrugated airfoils [19]. Furthermore, flat plates have also been used to study control-related problems such as the active control for providing lift enhancement [20] or determining the frequency of vortex shedding [21], even at ultra-low *Re* [22, 23]. Moreover, flat plates have also attracted the attention of other branches of engineering and have been used, for example, to analyze the behavior of bridges [24] or to correlate the turbulence intensity and length scale with the unsteady lift force in an atmospheric boundary layer flow [25].

One of the most significant parameters to characterize the aerodynamics of any object is the lift coefficient, C_L and its linear variation with the angle of attack, α. Thus, obtaining the lift coefficient slope ($C_{L\alpha}$) is essential for any wing design. Comparisons between flat plates and other aerofoils such as NACA0012 have been carried out, finding similar lift coefficients at angles of attack equal to 6.5° [10]. It is worth mentioning that we chose a flat plate wing model to study the dependence of $C_{L\alpha}$ for the sake of simplicity since some other symmetrical aerofoils such as NACA0012 would lead to multiple slopes at low *Re* and low angles of attack [10] together with some non-linearities manifested in the form of the presence of negative lift for positive attack angles close to 0 [26]. Some authors analyzed the influence on the lift coefficient slope showing that it depends not only on *Re* but also on the aspect ratio for low *Re* in a NACA0012 wing model. Specifically, a correlation was proposed to estimate the lift coefficient slope for each aspect ratio and Reynolds number pair comparing results obtained from several authors [27].

Focusing on the case of a flat plate, the first approximation was theoretically predicted for the case of a two-dimensional object at high *Re*, the so-called potential theory. The slope of the lift coefficient,

$$C_{L\alpha} = \left.\frac{dC_L}{d\alpha}\right|_{\alpha_0} \approx a_0, \tag{1}$$

being a_0=2π at small angles of attack in the inviscid limit. Kutta-Joukowsky theorem has been also proved to obtain the circulation experimentally but for lower *Re* [28]. The second correction to this thin-airfoil theory taking into account the wing aspect ratio, and using Prandtl's lifting line for a rectangular wing with elliptic loading showed that

$$C_{L\alpha} = \frac{a_0}{\left(1 + \frac{a_0}{\pi AR}\right)}, \tag{2}$$

instead of a_0 [29, 30]. A rectangular wing with a more general lift loading provides similar results,

$$C_{L\alpha} = \frac{a_0}{\left(1 + \frac{a_0}{\pi AR}(1 + \delta)\right)}, \tag{3}$$

with δ constant of value approximately $\delta \approx 0.024$. This simple approximation takes into account the induced lift, and also that the flow in a finite flat plate remains attached to the leading edge and sides at small angles attack [31]. In fact, it is reported that there are two important ranges of

angles of attack differing by the extent of flow separation on the upper surface [32]. At angles of attack below about 8°, flow separation and reattachment occur, and the well-known thin-airfoil theory is adequate for predicting the lift and normal force on the plate. Similar results were noted for other thin airfoil sections. Conversely, for angles of attack above about 8°, flow separation at four sides forms a complex wake structure. Following with other theoretical correlations, and assuming an elliptic span loading Helmbold derived the third equation that is widely used for wing design

$$C_{L\alpha} = \frac{a_0}{\sqrt{1 + \left(\frac{a_0}{\pi AR}\right)^2} + \frac{a_0}{\pi AR}}, \tag{4}$$

for a finite flat-plate or low-aspect-ratio straight wings [33]. However, none of these expressions take into account the dependence of the lift with the pair *Re*, *AR* since they are typically used in the limit of high *Re*. The present research provides a general expression for the slope of the lift coefficient for moderate *Re* and for *AR* between 1 and 8.

The curve lift slope $C_{L\alpha}$ depends experimentally at low *Re* on several parameters such as the Reynolds' own value, *AR* [5, 34], roughness surface of the aerofoil ϵ [1], turbulence intensity $\%I$ [35], thickness and edge shape of the aerofoil [36, 37], and Mach number *M* [38], among others. The pioneer experiment for a large flat plate wing model (*AR*=14.1) with small and high angles of attack was carried out in 1927 [39]. More recently, the first relevant (experimental) study characterizing the aerodynamics of different flat and cambered plane wings at moderate Reynolds number ($60 \times 10^3 \leq Re \leq 200 \times 10^3$) and low aspect ratio was presented in 2000 by Pelletier and Mueller [40] and it is considered a key reference in this area of study. In this work, they provide results for flat plate aerodynamic coefficients in infinite (2D) and finite wings (3D). This investigation was later extendend focusing on the lowest *AR* in Torres and Mueller [41]. Later, other authors have reported more information regarding low-aspect-ratio cases at low *Re* not only experimentally but also through numerical simulations [4, 19]. Other authors have pointed out experimentally how the maximum lift decreases as *AR* increases [42, 37]. Finally, Ananda *et al.* [43] measured the aerodynamic coefficients of different rectangular and tapered plate wing models at low Reynolds numbers taking into account the three-dimensional phenomena in the range of *AR* between 2 and 5, finding important differences with the two-dimensional case.

The wide range of applications for smaller dimensions makes the understanding of the aerodynamics at low *Re* numbers crucial. Due to the importance of the lift coefficient in general and of the slope of the lift coefficient in particular, we have designed different experiments to be able to propose a correlation taking into account not only *AR* but also *Re* for the simplest model of an airfoil, a flat plate. Using this correlation would facilitate the dimensioning of wings for aerial vehicles with working conditions in the low *Re* regime. Therefore, this work could be the base to extend the results to other more realistic aerodynamic profiles.

2. Experimental Arrangement

We have measured the lift coefficient in rectangular flat plates in the pre-stall region and small values of geometric thickness to chord ratio (t/c=0.0133), along with low turbulence levels under subsonic conditions (Mach numbers below 0.06). The experimental tests were performed using rounded rectangular aluminum plates in the closed low-speed wind tunnel of the Microaerial Vehicle Laboratory at the University of Malaga. We mainly employed the same setup described in [26] but using rectangular plates as wing models. We have repeated the main characteristics of the experimental setup to facilitate reading.

Re	$40e3$	$80e3$	$120e3$	$160e3$	$200e3$
Turb. (%)	0.8	0.5	0.35	0.35	0.35

Table 1: Measured turbulence level using Hot-Wire Anemometer for each Reynolds number used for the study.

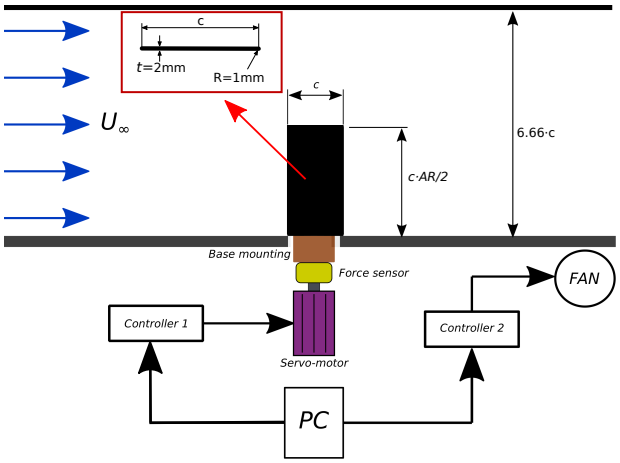

Figure 1: Experimental setup scheme. The inset represents the cross-section of the flat plate to highlight the rounded leading and trailing edges.

The wind tunnel has a 4 m long closed test section, 1x1 m cross-section and free stream velocity from $U_\infty = 4$ *to* 40 m/s. Each experiment was characterized by its chord-based Reynolds number Re, defined as

$$Re = \frac{U_\infty \cdot c}{\nu}, \tag{5}$$

where ν is the kinematic viscosity at the wind tunnel conditions. We used rectangular plates with chord of $c = 150$ mm and thickness of $t = 2$ mm. The length of the profiles, l, varies from 75mm to 600 mm, so the aspect ratio $AR = 2l/c$ is between 1 and 8. The turbulence intensity has been measured using hot-wire anemometry obtaining values of turbulence intensity lower than 0.8% for all the studied Reynolds (see Table 1).

The aerodynamic forces were measured using a precise 6 axis force/torque sensor ATI FTD-GAMMA SI-32-2.5 sensor of accuracy ± 0.006 N. This force sensor was fixed to a stepper motor to control the angle of attack, and the assembly has been screwed to the floor outside the wind tunnel to avoid structural vibration noise that would affect the walls of the test section. The plate was attached firmly to an aluminium base, which was joined to the top of the force sensor and leveled with the floor of the wing tunnel. A scheme of the experimental setup is shown in figure 1.

To use force measurements to calculate lift and drag coefficients, some considerations are needed. Since the z axis of the transducer has the direction of the gravity force, the aerodynamic forces only act in the (x, y)-plane. The wing chord was aligned with the x-axis of the force sensor and the system is turned rigidly with it, thus creating a local coordinate system centered in the wing. To obtain the forces in a global coordinate system aligned with the wind direction, (that is to say, to compute the lift and drag forces), the following transformation was used:

$$F_{xD} = F_x \cos(\alpha) - F_y \sin(\alpha)\,, \tag{6}$$

$$F_{yL} = F_x \sin(\alpha) + F_y \cos(\alpha)\,. \tag{7}$$

In these equations, we have already subtracted the offset of the force signals, F_x and F_y. The non-dimensional forces in the global coordinate system are given by

$$C_D = \frac{2F_{xD}}{\rho U_\infty^2 A}\,, \qquad C_L = \frac{2F_{yL}}{\rho U_\infty^2 A} \tag{8}$$

where ρ is the air density at wind tunnel conditions, and A is the aerodynamic area as a rectangular model $A = c^2 \cdot AR/2$ (see figure 1).

A servomotor at 10000 steps per revolution controlled the angles of attack during the experiments allowing small variations in α. The measurements were taken with steps of 1°. For each angle of attack, the force was obtained by collecting data for 8 seconds. Each experiment was repeated three times for each range of angles of attack to check repeatability and to obtain the average value and standard deviation of lift and drag curves with α.

We did not observe any relevant tunnel blockage effects since it had a maximum value of 1.36% for $AR = 8$. The angle of attack, lift and drag corrections due to curvature streamlines are computed using the formulas provided by Barlow *et al.* [44] and by McAlister and Kenneth [45]. The angle correction is almost zero and thus the lift corrections. The drag correction is found to be at most 1% of its value around $\alpha = \pm 15°$ and decreasing as the angle of attack is decreasing. These values are consistent with the junction study presented by Bernstein & Hamid [46] reported also in Malik [47] for the case of a NACA 0015 but in that case the influence the corrections are amplified due to the higher *Re*. In our case, all these corrections are so small that were neglected.

3. Experimental measurements

3.1. Validation

A flat plate of $AR = 2$ at $Re = 160\times10^3$ was used to compare the results with the well-known, established results of Pelletier and Mueller [40]. In Fig 2, lift and drag coefficients versus the angle of attack are compared with those provided by Pelletier and Mueller [40] for a flat plate of $AR = 2$ at $Re = 140 \times 10^3$ finding good agreement with our results. Additionally, data from Fedoul *et al.* [15] with a slightly higher *Re* (nearest to our value) are also superposed as second validation.

3.2. Results

We performed experiments to measure C_L on flat plates for different angles of attack, *Re*, and *AR*. Figures 3(a)-(e) display C_L for five different *Re* in the range of $40 \times 10^3 \leq Re \leq 200 \times 10^3$. Each of them contains results corresponding with four different *AR* in the range of $1 \leq AR \leq 8$ with a resolution $\Delta\alpha = 1°$. For small *AR*, the value of C_L is increasing with approximately the same rate of change for every angle of attack. However, for bigger *AR*, there exist two different slopes, a steeper one for the range of small angles of attack and a softer one for the bigger angles of attack. See for example 3(a) focusing on $AR = 8$, purple curve, where the change in slope is evident around $\alpha \approx \pm 8°$. Also, the reader can observe that the measurements show a more

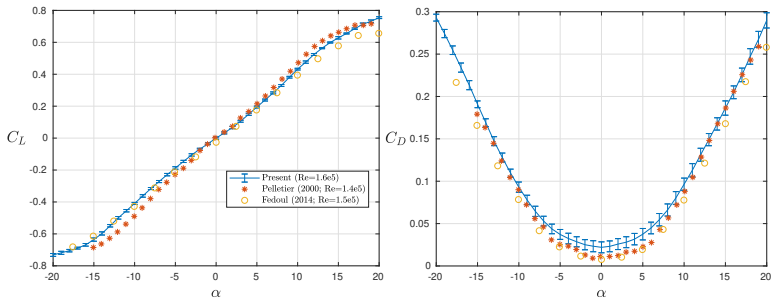

(a) (b)

Figure 2: Validation of force measurements for a flat plate at $Re = 160 \times 10^3$ and $AR = 2$ comparing with Pelletier & Mueller [40] at $Re = 140 \times 10^3$ and Fedoul *et al.* [15] 150×10^3.

significant error for the case of $Re = 40 \times 10^3$ and small AR since the forces in these cases are close to the lower limit of our measuring equipment.

Since the curves are approximately linear in the range of small angles of attack, we can calculate their slope, $C_{L\alpha}$, using a linear fit as proposed by [27]. Therefore, we calculate the slope for the range of smaller α ($-7° \leq \alpha \leq 7°$) for each Re, AR pair. Note that in this range, the data is so linear that the same value of $C_{L\alpha}$ is obtained when computing a second-degree polynomial approximation to the lift and considering $C_{L\alpha}$ to be the linear coefficient as reported by [41]. Figure 4(a) shows all the computed $C_{L\alpha}$ with respect to Re along with the errors based on the standard deviation of three experiments. We can observe how $C_{L\alpha}$ increases with the aspect ratio and with Re, but the influence of Re on the variation of $C_{L\alpha}$ is less noticeable in the figure for the smallest Re values. To visualize better this influence, figure 4(b) represents all the measured slopes with respect to AR. The increment of $C_{L\alpha}$ when increasing the aspect ratio and Re is clear. The same weak influence of the Reynolds numbers on $C_{L\alpha}$ and the growth of $C_{L\alpha}$ with AR has been reported previously by Ananda *et al.* [43], showing a precise experimental methodology again.

4. Correlation between $C_{L\alpha}$, aspect ratio and Re

As mentioned above, the lift slope is a key criterion for any initial wing design. Therefore, we aim to find a correlation to obtain $C_{L\alpha}$ as a function of the aspect ratio and the Reynolds number. The literature presents several studies obtaining this slope for specific AR and Re pairs but, to the best of our knowledge, no one has offered a correlation including both parameters. As mentioned in the introduction section, there are several correlations for the lift slope depending only on the AR and being valid for high Re. Following the idea of Prandt's lifting line but including the influence of Re for moderate values, we propose the following correlation:

$$C^*_{L\alpha} = \left(\frac{2\pi}{1 + \alpha_1 * AR^{-1}}\right)\left(\frac{\alpha_2}{1 + 10^6/Re}\right)^{1/5} \tag{9}$$

with $\alpha_1 = 5.21$ and $\alpha_2 = 14.61$.

Figure 5 represents in dashed lines the computed $C_{L\alpha^*}$ using the correlation superposed with the measured values shown in figure 4 to follow the trends of the correlation in equation (9).

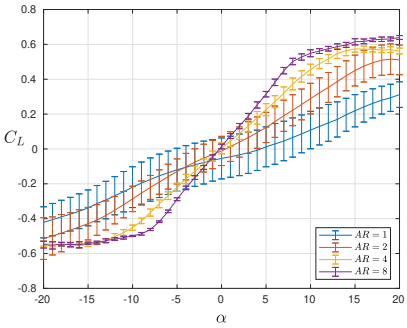

(a) $Re = 40 \times 10^3$

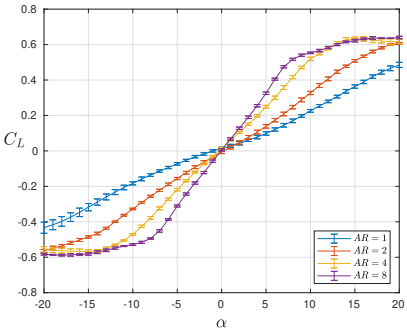

(b) $Re = 80 \times 10^3$

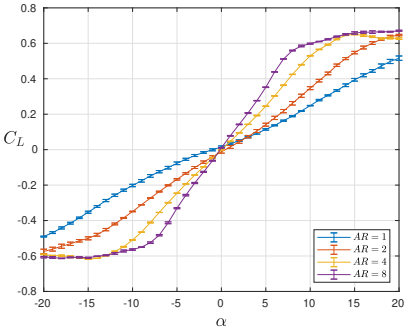

(c) $Re = 120 \times 10^3$

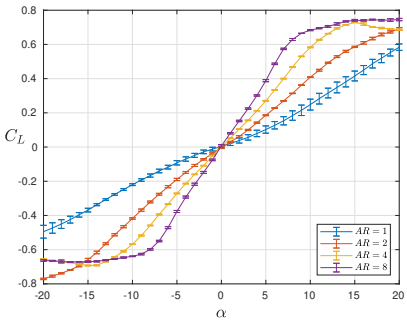

(d) $Re = 160 \times 10^3$

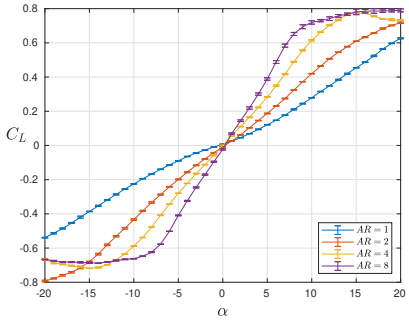

(e) $Re = 200 \times 10^3$

Figure 3: Variation of C_L versus α for different AR for the following cases: (a) $Re = 40 \times 10^3$,(b) $Re = 80 \times 10^3$, (c) 120×10^3, (d) $Re = 160 \times 10^3$, (e)$Re = 200 \times 10^3$.

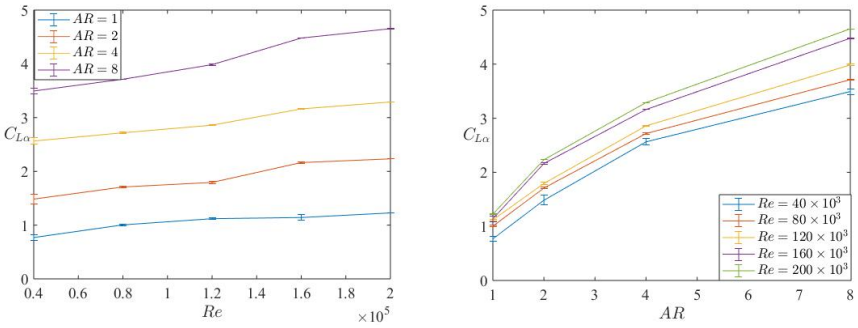

(a) (b)

Figure 4: Variation of the measured $C_{L\alpha}$ with respect to Reynolds number (a) and aspect ratio (b).

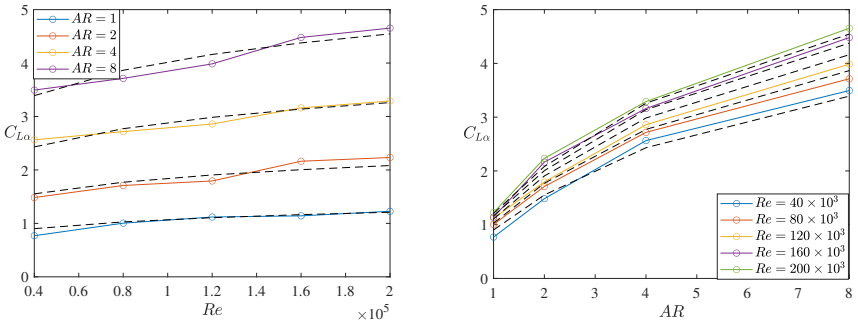

(a) (b)

Figure 5: Variation of the measured $C_{L\alpha}$ with respect to Reynolds number (a) and aspect ratio (b). Superposed in dashed lines the computed $C_{L\alpha^*}$ values using the correlation in equation (9).

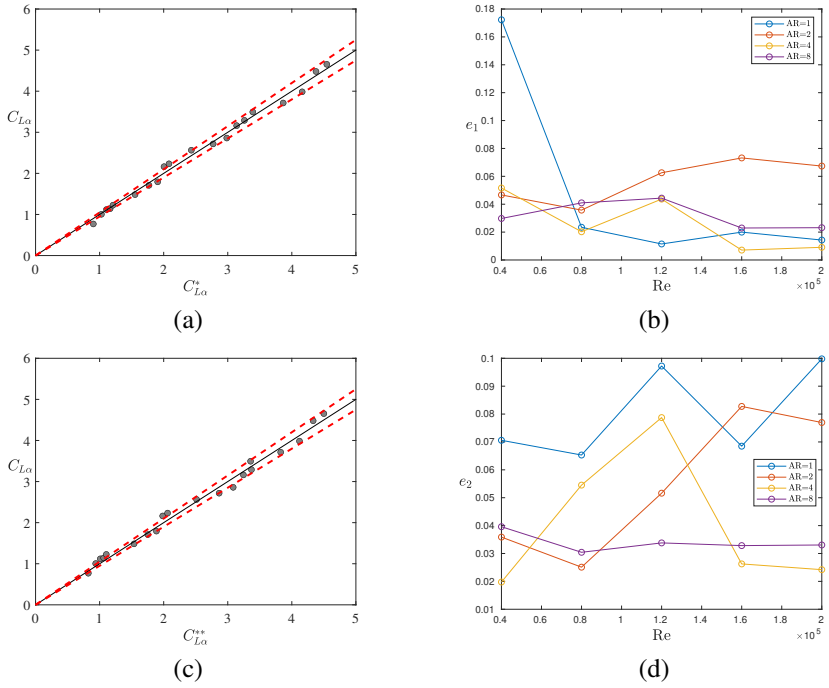

Figure 6: Computed $C^{*}_{L\alpha}$ and $C^{**}_{L\alpha}$ using the correlations in equations (9)-(10) versus measured $C_{L\alpha}$ obtained directly as the slope for different Re and AR, in (a)-(c) respectively. Relative error when computing $C^{*}_{L\alpha}$, $e_1 = |\frac{C^{*}_{L\alpha} - C_{L\alpha}}{C_{L\alpha}}|$, (b) and relative error when computing $C^{**}_{L\alpha}$ (d) for each Re, AR value.

To quantify the accuracy of the proposed correlation, figure 6 (a) displays $C_{L\alpha}$ obtained directly as the slope for every Re and AR together with the computed slope, using the proposed correlation, $C^{*}_{L\alpha}$, showing excellent agreement. Figure 6 (a) also presents two red dashed lines, which represent the confidence interval of 5% to help the visualization. When computing the error for each Re, AR, and averaging them, we obtain a mean error of 4.1%. Thus, we can conclude that the proposed correlation is a good approximation for $C_{L\alpha}$ for a flat plate in our study range.

Furthermore, we have analyzed the errors for each Re, AR pair individually. Figure 6 (b) shows the relative error for each $C^{*}_{L\alpha}$ when comparing it with $C_{L\alpha}$ directly measured in each experiment ($e_1 = |\frac{C^{*}_{L\alpha} - C_{L\alpha}}{C_{L\alpha}}|$). It is noticeable how the accuracy of the correlation, even though is good for every value, it is not consistent for all the aspect ratios having peaks for some Re, AR pairs and extremely good agreement for some others (including some values with an error below 2%). Note that there is one value showing a relatively high error for $Re = 40 \times 10^3$ and $AR = 1$, but that is also the value with more uncertainties in the measurements. If that measured value is neglected, the average error would be even smaller. In general, the error decreases as AR and Re increase.

Focusing on the literature for small aspect ratio wings, we could also consider the idea of computing a correlation related with the value of $C_{L\alpha}$ proposed by Helmbold [33] for a finite flat-plate low-aspect-ratio straight wings, see equation (4). Therefore, we provide a second correlation of the form of:

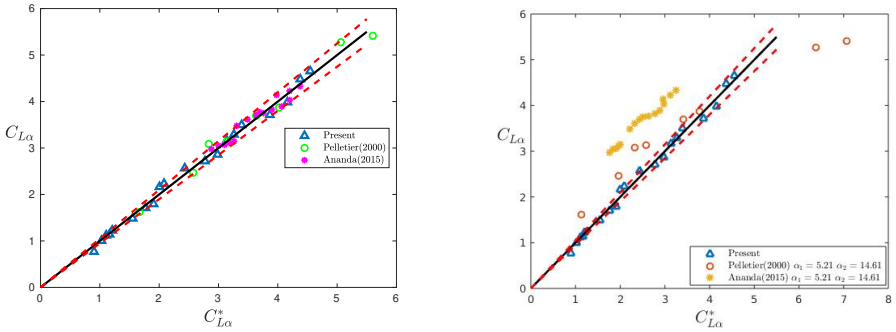

(a) (b)

Figure 7: Computed $C_{L\alpha^*}$ using the correlation in equation (9) with (a) their corresponding parameters α_1 and α_2 for each author and (b) $\alpha_1 = 5.21$ and $\alpha_2 = 14.61$ versus the measured $C_{L\alpha}$ obtained directly as the slope for different Re and AR for different authors.

$$C^{**}_{L\alpha} = \left(\frac{\alpha_1}{\sqrt{1 + [\alpha_1/(\pi AR)]^2} + \alpha_1/(\pi AR)} \right) \left(\frac{\alpha_2}{1 + 10^6/Re} \right)^{1/5} \tag{10}$$

and fitted the results with $\alpha_1 = 3.79$ and $\alpha_2 = 44.53$.

Figure 6 (c) displays the comparison between the estimated and measured $C_{L\alpha}$ obtaining a good agreement. In fact, this correlation is only slightly worst than the previous one, with an average error of 5.23%. However, when looking at the details of the error for each Re, AR pair (see figure 6 (d)), we can appreciate how the error is less consistent for each AR. Furthermore, for the highest Re, the errors of the two smaller AR are bigger than for $AR = 4$ and $AR = 8$. Therefore, for the following, we have used the correlation defined by eq. (9).

5. Comparison with previous results presented in the literature

We have presented a correlation in the range of $40 \times 10^3 \leq Re \leq 200 \times 10^3$ and $1 \leq AR \leq 8$ derived from our own measurements. There are two other studies in literature by Pelletier and Mueller [40] and Ananda *et al.* [43] which contain several measured values in the same range of Re and AR. We have used our correlation to fit their data and we have obtained $\alpha_1 = 2.35$ and $\alpha_2 = 4.58$ for Pelletier and Mueller [40] and $\alpha_1 = 2.20$ and $\alpha_2 = 11.15$ Ananda *et al.* [43]. Figure 7 (a) represents $C_{L\alpha}$ versus $C^*_{L\alpha}$ for both of those studies together with our data. In all cases, a good agreement is clear. Thus, we can conclude that all of them follow the same kind of dependence with AR and Re. Results of computed values using our experimental parameters $\alpha_1 = 5.12$ and $\alpha_2 = 14.61$ are shown for quantitetively comparison in figure 7(b). The differences in the correlation parameters are expected since the actual value of $C_{L\alpha}$ slightly depends on some other characteristics such as the roughness, thickness and edge shape of the aerofoil of the wing that are not considered explicitly in the correlation. These characteristics are different in each of the three studies. For example, our flat plates have both endings rounded equally, but the plates considered in Pelletier and Mueller [40] have rounded leading edge and tapered edge and the ones in Ananda *et al.* [43] are both rounded but not symmetrically. See table 2 for a summary of the other main characteristics of each study. Note also that the study of Pelletier and Mueller [40]

Study	thickness t/c	%I of turbulence	Re	AR
Present	0.0133	$I\% \leq 0.8$	$40 - 200 \times 10^3$	$1 \leq AR \leq 8$
Pelletier and Mueller (2000)	0.0193	$I\% \leq 0.05$	$80 - 140 \times 10^3$	$1 \leq AR \leq \infty$
Ananda *et al.* (2015)	0.026	$I\% \leq 0.1$	$60 - 160 \times 10^3$	$2 \leq AR \leq 5$

Table 2: Main parameters from various studies.

includes 2D values, outside our study range. We have also used our correlation to analyze those values, corresponding to the higher circle values in figure 7 (a), and it correlates them correctly.

6. Conclusions

We have measured the lift coefficient for several flat plates with different aspect ratios varying the Reynolds number in a range of $40\times10^3 \leq Re \leq 200\times10^3$ and the aspect ratio $1 \leq AR \leq 8$. For small angles of attack, the variation of the lift coefficient is linear and, therefore, it can be defined simply by knowing the slope of the function $C_{L\alpha}$. We have proposed a correlation to provide this slope for different Re and AR that contains two free parameters: α_1, α_2. The proposed correlation contains two parts, one that modifies the value of $C_{L\alpha}$ taking into account the use of finite wings and that behaves similarly to the results predicted by Prandtl's lifting line theory. The second part only depends on the Reynolds number. The proposed correlation is able to predict the value of $C_{L\alpha}$ within an average error of 4.1% in the studied range. Lastly, we have shown how we could extrapolate the values of other authors following the same kind of fitting. This correlation provides accurate results, even outside the AR study range.

We believe that this same type of semi-empirical correlations can be extended to be used in more realistic wing profiles, and in addition, are capable of describing its behavior up to the limit situations of 2D flow ($AR \to \infty$) in some cases. Finally, the dependence of the correlation with respect to the Reynolds number is completely heuristic, and leaves open the possibility of obtaining physical scale laws for the calculation of this slope dependence with respect to Re, together with a plausible theoretical explanation of the exponent 1/5.

Acknowledgments

This research has been supported by the grant from the Ministerio de Economia y Competitividad of Spain (Grant No. DPI2016-76151-C2-1-R).

References

[1] D. J. Pines, F. Bohorquez, Challenges facing future micro-air-vehicle development, Journal of Aircraft 43 (2) (2006) 290–305.

[2] J.-M. Moschetta, The aerodynamics of micro air vehicles: technical challenges and scientific issues, International Journal of Engineering Systems Modelling and Simulation 6 (2014) 134–148.

[3] E. N. Barmpounakis, E. I. Vlahogianni, J. C. Golias, Unmanned aerial aircraft systems for transportation engineering: Current practice and future challenges, International Journal of Transportation Science and Technology 5 (2016) 111–122.

[4] P. Cosyn, J. Vierendeels, Numerical investigation of low-aspect-ratio wings at low Reynolds numbers, Journal of Aircraft 43 (3) (2006) 713–722.

[5] L. Traub, Aerodynamic impact of aspect ratio at low Reynolds number, Journal of Aircraft 50 (2) (2013) 626–634.

[6] X. Ortiz, D. Rival, D. Wood, Forces and moments on flat plates of small aspect ratio with application to PV wind loads and small wind turbine blades, Energies 8 (2015) 2438–2453.
[7] K. Zhang, S. Hayostek, M. Amitay, W. He, W. Theofilis, T. K., On the formation of three-dimensional flows over finite-aspect-ratio wings under tip effects, Journal of Fluid Mechanics 895. doi:10.1017/jfm.2020.248.
[8] C. del Pino, P. L., M. Felli, R. Fernandez-Feria, Structure of trailing vortices: Comparison between particle image velocimetry measurements and theoretical models, Physics of Fluids 23 (2011) 013602.
[9] J. H. García-Ortiz, A. Domínguez-Vázquez, J. Serrano-Aguilera, L. Parras, C. del Pino, A complementary numerical and experimental study of the influence of reynolds number on theoretical models for wingtip vortices, Computers & Fluids 180 (2019) 176 – 189.
[10] T. Lee, Y. Y. Su, Low Reynolds number airfoil aerodynamic loads determination via line integral of velocity obtained with particle image velocimetry, Experiments in Fluids 53 (2012) 1177–1190.
[11] R. Nakayama, Y. Nakamura, Y. Ohya, S. Ozono, A numerical study on the flow around flat plates at low Reynolds numbers, Journal of Wind Engineering and Industrial Aerodynamics 46 (1993) 255–264.
[12] L. Rosenhead, The lift on a flat plate between parallel walls, Proceeding Royal Society London A 132 (1931) 127–152.
[13] T. H. Havelock, Flow over a flat plate with uniform inlet and incident coherent gusts, Proceeding Royal Society London A 166 (1938) 178–196.
[14] M. G. Savage, G. L. Larose, An experimental study of the aerodynamic influence of a pair of winglets on a flat plate model, Journal of Wind Engineering and Industrial Aerodynamics 91 (2003) 113–126.
[15] F. Fedoul, L. Parras, C. del Pino, R. Fernandez-Feria, Experimental study of the aerodynamic characteristics of a low-aspect-ratio flat plate array in a configuration of interest for a tidal energy converter, Journal of Fluids and Structures 48 (2014) 487–496.
[16] B. Wu, Q. Wang, H. Liao, Y. Li, M. Li, Flutter derivatives of a flat plate section and analysis of flutter instability at various wind angles of attack, Journal of Wind Engineering and Industrial Aerodynamics 196 (2020) 104046.
[17] Z. Zhang, J. P. Hubner, A. Timpe, L. Ukeiley, Y. Abudaram, P. Ifju, Effect of aspect ratio on flat-plate membrane airfoils, 50th AIAA Aerospace Sciences Meeting including the New Horizons Forum and Aerospace Exposition (2012) 1–15.
[18] H.-T. Yu, L. P. Bernal, Effects of pivot location and reduced pitch rate on pitching rectangular flat plates, AIAA Journal (2016) 1–17.
[19] J. T. Murphy, H. Hu, An experimental study of a bio-inspired corrugated airfoil for micro air vehicle applications, Experiments in Fluids 49 (2010) 531–546.
[20] Z. Wnag, I. Gursul, Lift enhancement of a flat-plate airfoil by steady suction, AIAA Journal 55 (2017) 1–18.
[21] J. M. Chen, Y.-C. Fang, Strouhal numbers of inclined flat plates, Journal of Wind Engineering and Industrial Aerodynamics 61 (1996) 99–112.
[22] W. E. Olmstead, D. L. Hector, The lift and drag on a flat plate at low Reynolds number via variational methods, Quarterly of Applied Mathematics 25 (1966) 415–422.
[23] I. Afgan, S. Benhamadouche, X. Han, P. Sagaut, D. Laurence, Flow over a flat plate with uniform inlet and incident coherent gusts, Journal of Fluid Mechanics 720 (2013) 457–485.
[24] G. L. Larose, F. M. Livesey, Performance of streamlined bridge decks in relation to the aerodynamics of a flat plate, Journal of Wind Engineering and Industrial Aerodynamics 69-71 (1997) 851–860.
[25] A. Jafari, F. Ghanadi, M. Arjomandi, M. J. Emes, B. S. Cazzolato, Correlating turbulence intensity and length scale with the unsteady lift force on flat plates in an atmospheric boundary layer flow, Journal of Wind Engineering and Industrial Aerodynamics 189 (2019) 218–230.
[26] J. Aguilar Cabello, P. Gutierrez-Castillo, L. Parras, C. del Pino, E. Sanmigul-Rojas, On the onset of negative lift in a symmetric airfoil at very small angles of attack, Physics of Fluids 32 (2020) 055107.
[27] S. Martínez-Aranda, A. García-González, L. Parras, J. Velázquez-Navarro, C. Del Pino, Comparison of the aerodynamic characteristics of the NACA0012 airfoil at low-to-moderate reynolds numbers for any aspect ratio, International Journal of Aerospace Sciences 4 (1) (2016) 1–8.
[28] S. D. Sharma, P. J. Deshpande, Kutta-Joukowsky theorem in viscous and unsteady flow, Experiments in Fluids 52 (2012) 1581–1591.
[29] H. Glauert, The Elements of Aerofoil and Airscrew Theory, Cambridge Univ. Press, London, 1947.
[30] J. D. Anderson, Fundamentals of Aerodynamics, McGraw-Hill, New York, 1947.
[31] D. Küchemann, A simple method for calculating the span and chordwise loading on straight and swept wings of any given aspect ratio at subsonic speeds, Research and Memoranda 2935 132 (1952) 1–54.
[32] B. H. Wick, Study of the subsonic forces and moments on an inclined plate of infinite span, NACA TN 3321 (1954) 1–25.
[33] H. B. Helmbold, Der unverwundene Ellipsenflügel als tragende fläche., Jahrbuch der Deutschen Luftfahrtforschung, R. Oldenbourg (Munich) (1942) I–111–I–113.
[34] T. LIneham, K. Mohseni, Leading-edge flow reattachment and the lateral static stability of low-aspect-ratio rectan-

gular wings, Physical Review Fluids 2 (2017) 113901.
[35] S. Watkins, S. Ravi, B. Loxton, The effect of turbulence on the aerodynamics of low Reynolds number wings, Engineering Letters 18 (2010) 1–6.
[36] S. Sunada, A. Sakaguchi, K. Karachi, Airfoil section characteristics at a low reynolds number, Journal of Fluids Engineering 119 (1997) 129–135.
[37] M. Shields, K. Mohsenii, Effects of sideslip on the aerodynamics of low-aspect-ratio low-Reynolds-number wings, AIAA Journal 50 (2012) 85–99.
[38] R. C. Frost, R. Rutherford, Der unverwundene Ellipsenflügel als tragende fläche, AIAA Journal (1963) 931–933.
[39] A. Fage, B. Johansen, On the flow of air behind an inclined flat plate of infinite span, Proceeding Royal Society London A 116 (1927) 170–197.
[40] A. Pelletier, T. J. Mueller, Low reynolds number aerodynamics of low-aspect-ratio, thin/flat/cambered-plate wings, Journal of Aircraft 37 (5) (2000) 825–832.
[41] G. E. Torres, T. J. Mueller, Low aspect ratio aerodynamics at low Reynolds numbers, AIAA Journal 42 (5) (2004) 865–873.
[42] M. Mizoguchi, Y. Yamaguchi, Aerodynamic characteristics of rectangular flat plate wings in low Reynolds number flows, Journal of the Japan Society for Aeronautical and Space Sciences 60 (2012) 121–127.
[43] G. Ananda, P. Sukumar, M. Selig, Measured aerodynamic characteristics of wings at low reynolds numbers, Aerospace Science and Technology 42 (2015) 392–406.
[44] J. B. Barlow, X. Rae, X. Pope, Low-Speed Wind Tunnel Testing, Chap 10, Wiley, New York, 1999.
[45] K. W. McAlister, NACA 0015 wing pressure and trailing vortex measurements, Vol. 3151, National Aeronautics and Space Administration, Office of Management , 1991.
[46] L. Bernstein, S. Hamid, On the effect of a swept-wingplate junction flow on the lift and drag, The Aeronautical Journal 99 (987) (1995) 293–305.
[47] A. Malik, Suppression of junction flow effects in half model wind tunnel testing, Ph.D. thesis, Loughborough University (2012).